JOURNAL OF SPACECRAFT AND ROCKETS
Vol. 32, No. 5, September–October 1995

Analysis of Close-Packed Brush-Fiber Interfaces for Spacecraft Thermal Management

K. O. Lund*
University of California, San Diego, La Jolla, California 92093-0411
and
G. E. Henschke† and T. R. Knowles‡
Energy Science Laboratories, Inc., San Diego, California 92121-2232

A new interpenetrating-brush thermal interface is analyzed and evaluated for application to space-based thermal management. The interface consists of fibers attached to oppositely facing substrates. Each fiber is attached to one or the other substrate but not both. Heat transfer occurs through conduction and radiant exchange between interpenetrating fibers of opposite substrates. Linearization of the radiation terms results in an analytical temperature distribution along the fibers. The thermal performance of the interface is expressed in terms of a thermal effectiveness and an effective conductance-length ratio, both of which depend on the radiation/conduction number. For thin enough fibers, the heat transfer approaches that of the case in which all fibers are attached to both substrates. A fiber length (parameter-dependent) for optimum heat transfer is identified and agrees with previously published results. Such interfaces offer both high thermal effectiveness and compliance and are well suited for internal and external spacecraft applications.

Nomenclature

A	= total x-sectional area of fibers on one side, m^2
A_b	= base (substrate) area, m^2
a	= single fiber (fin) cross-sectional area, m^2
d	= fiber diameter, m
$\mathcal{E}$	= effectiveness factor
F	= view factor
$\mathcal{F}$	= transfer function
h	= unit surface conductance, W/m^2 · K
K	= thermal conductance, kA/L_d, W/K
k	= thermal conductivity, W/m · K
L	= length, m
P	= total fiber (fin) perimeter, m
p	= single fiber (fin) perimeter, m
Q	= rate of heat transfer, W
q	= heat flux, W/m^2
R	= thermal resistance, K/W
T	= temperature, K
t	= plane fin thickness, m
U	= overall interface conductance, W/m^2 · K
V	= volume, m^3
X	= axial coordinate, m
x	= nondimensional axial coordinate, X/L_d
β	= radiation/conduction number
ε	= emissivity
η	= efficiency factor
θ	= nondimensional "excess" temperature
κ	= conductance ratio, $K_1/K_2 + K_2/K_1$
λ	= effective conductance length ratio, L_e/L_d
σ	= Stefan–Boltzmann constant
ϕ	= fractional length of fiber penetration, L_d/L_{fe}
χ	= volume fraction, $V_f/V_b = A/A_b$

Subscripts

b	= base of fiber (fin) attachment
d	= depth of interpenetration
e	= effective value
f	= fiber or fin
i, 1, 2	= side i, 1, 2 of interface
m	= mean or average
Q	= maximum heat transfer
R	= reference
r	= radiation

Introduction

A PREVALENT problem in thermal management is the resistance associated with interfaces and joints.[1,2] In vacuum applications such as the external space environment, conventional thermal interface greases have limited use because of evaporation and migration from the interface, and clean surfaces pressed together tend to make contact at a few special points and cold-weld together. Interleaving, plane fin structures have been developed for specific spacecraft applications, in one case using complicated clamping of the interleaving fins,[3] and in another relying on radiation between the fins.[4] The thermal performance of the latter design can be improved by using more highly conductive, highly dispersed materials. In this study we analyze interpenetrating fiber brush structures to guide the design for high-conductance joints.

We consider an extension of the interleaving plane fin design,[4] in which the metal fins (typically ~1 mm thick) are replaced with a large number of high-thermal-conductivity carbon fibers (typically ~10 μm in diameter). The interpenetrating fiber structure is illustrated schematically in Fig. 1.

The present analysis is in terms of radial radiation heat transfer between fibers but applies to plane fins as well. This neglection of axial radiative components, compared to the radial components, is considered valid for close-packed structures where the fiber lengths are much greater than the average fiber-to-fiber separation, and for high thermal conductivity ($\beta \leq 1$). In addition, conductive transfer between fibers (fins) through an intervening conductive medium can be treated the same way by appropriate interpretation of $\mathcal{F}$ and β. In practice, it is likely that some of the fibers from opposite substrates will touch, and thus increase the heat transfer; in this case the results presented here are regarded as lower bound for the interface rate of heat transfer, which practical embodiments may exceed.

Presented as Paper 94-0450 at the AIAA 32nd Aerospace Sciences Meeting, Reno, NV, Jan. 10–13, 1994; received Feb. 9, 1994; revision received March 3, 1995; accepted for publication April 11, 1995.

*Assistant Research Engineer, Department of Applied Mechanics and Engineering Science.
†Engineer.
‡Principal Scientist.

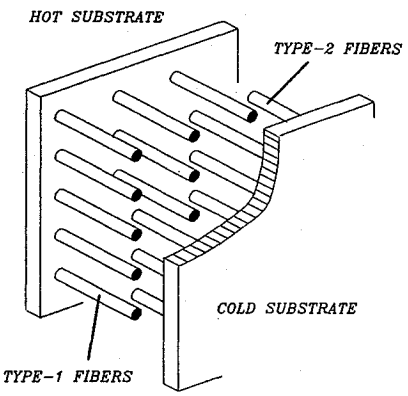

Fig. 1 Schematic structure of interpenetrating-brush heat exchanger.

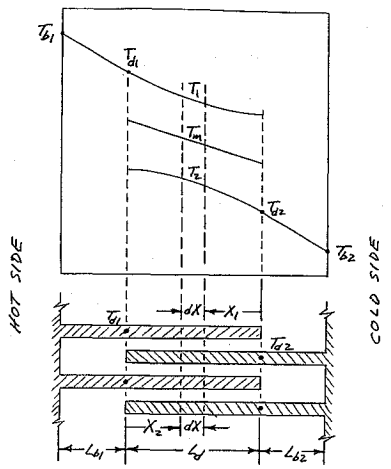

Fig. 2 Coordinates and temperatures used in brush-fiber heat transfer calculations.

Problem Formulation

Heat exchange from the hot side to the cold side of the interface occurs by axial conduction through the hot fibers attached to the hot side (here called type-1 fibers), followed by radiation (or radial conduction) from the hot to the cold fibers, and axial conduction through the cold fibers attached to the cold side (here called type-2 fibers). Where there is interpenetration of the two types of fibers (which may or may not be identical in structure and properties), the temperatures vary continuously along the length of the fibers, as shown in Fig. 2.

For the radiation model we consider diffuse-gray surfaces and limit investigation to fiber interpenetration depths L_d that are large compared to the effective gap separating the fibers, so that radiation exchange occurs primarily in the radial direction. Because the identical fibers attached to one side have the same temperature distribution and properties, the totality of such fibers represent one surface of the radiation enclosure. Thus the radiant exchange model is that of a two-surface enclosure.

Consider, as in Fig. 2, a differential length of the interpenetration region where radiation occurs from type-1 fibers at local temperature $T_1(X_1)$ to type-2 fibers at temperature $T_2(X_2)$, at that axial location. Under these conditions, the rate of radiative heat transfer per unit length may be written as

$$q_{12} = P_1 \mathcal{F}_{12} \sigma \left(T_1^4 - T_2^4\right) \tag{1}$$

where $\mathcal{F}_{12}$ is the effective transfer function for radiation emitted at surface 1 and absorbed at surface 2. For example, for plane fins, and larger fibers or rods,[5]

$$\frac{1}{P_1 \mathcal{F}_{12}} = \frac{1-\varepsilon_1}{P_1 \varepsilon_1} + \frac{1}{P_1 F_{12}} + \frac{1-\varepsilon_2}{P_2 \varepsilon_2} \tag{2}$$

Thus, for plane fins with equal emissivities we have $\mathcal{F}_{12} = \varepsilon/(2-\varepsilon)$, whereas for rods (with $F_{12} = 0.5$), $\mathcal{F}_{12} = \varepsilon/2$. For small (micron-size) fibers, exact determination of the transfer function would involve multiple-scattering calculations, which are beyond the scope of the present article. However, the present analysis is carried forth in terms of $\mathcal{F}_{12}$, whatever its value.

With this model, energy balances on the type-1 and type-2 fibers yield

$$k_1 A_1 \frac{d^2 T_1}{dX_1^2} = P_1 \mathcal{F}_{12} \sigma \left(T_1^4 - T_2^4\right) \tag{3}$$

$$k_2 A_2 \frac{d^2 T_2}{dX_2^2} = P_2 \mathcal{F}_{21} \sigma \left(T_2^4 - T_1^4\right) \tag{4}$$

subject to the insulated-tip conditions

$$\frac{dT_1(0)}{dX_1} = 0, \qquad \frac{dT_2(0)}{dX_2} = 0 \tag{5}$$

and specified penetration-depth temperatures

$$T_1(L_d) = T_{d1}, \qquad T_2(L_d) = T_{d2} \tag{6}$$

In these equations the intermediate temperatures T_d are not really known, but are related to the boundary temperatures T_b as shown in Fig. 2. However, once a solution is obtained in terms of the T_d, it can be related to the boundary temperatures. In terms of these variables, the overall rate of heat transfer is given by

$$Q = k_1 A_1 \frac{dT_1(L_d)}{dX_1} = -k_2 A_2 \frac{dT_2(L_d)}{dX_2} \tag{7}$$

Because of reciprocity, the sum of Eqs. (3) and (4) yields the following characteristic of the conduction–radiation system, similar to that in a previous investigation[6]:

$$k_1 A_1 \frac{d^2 T_1}{dX_1^2} + k_2 A_2 \frac{d^2 T_2}{dX_2^2} = 0 \tag{8}$$

Hence, with the mean temperature defined by

$$T_m = \frac{K_1 T_1 + K_2 T_2}{K_1 + K_2} \tag{9}$$

and application of Eqs. (5) and (7), the mean temperature is the following linear function of position (as shown in Fig. 2):

$$T_m(X_1) = T_m(0) + \frac{Q}{K_1 + K_2} \frac{X_1}{L_d} \tag{10}$$

Therefore, determination of the slope of the mean temperature is important, as this establishes Q, the overall rate of heat transfer from side 1 to side 2 of the interface.

In terms of the radiation heat transfer coefficient

$$h_r = \sigma \left(T_1^2 + T_2^2\right)(T_1 + T_2) \approx \sigma \left(T_{1b}^2 + T_{2b}^2\right)(T_{1b} + T_{2b}) \tag{11}$$

Eqs. (3) and (4) may be written in their linearized forms

$$k_1 A_1 \frac{d^2 T_1}{dX_1^2} = P_1 \mathcal{F}_{12} h_r (T_1 - T_2) \tag{12}$$

$$k_2 A_2 \frac{d^2 T_2}{dX_2^2} = P_2 \mathcal{F}_{21} h_r (T_2 - T_1) \tag{13}$$

These forms are considered adequate approximations, since the design objective for the interface is to reduce the overall temperature drop as much as practicable, and they lead to convenient analytical solutions.

It should be observed that Eqs. (12) and (13) also describe interface heat transfer where there is an intervening conductive medium (say a liquid) between the two types of fibers. In this case the transfer function and heat transfer coefficient are associated with a geometric shape factor for radial conduction.

Solution of Equations

For the solution of the above equations it is convenient to introduce the following "excess" temperatures:

$$\theta_1 = \frac{T_1 - T_m}{T_R} = \frac{K_2}{K_1 + K_2}\frac{T_1 - T_2}{T_R} \tag{14}$$

$$\theta_2 = \frac{T_m - T_2}{T_R} = \frac{K_1}{K_1 + K_2}\frac{T_1 - T_2}{T_R} \tag{15}$$

where the definition (9) was used for the second equality. Clearly the excess temperatures are proportional:

$$K_2\theta_2 = K_1\theta_1 \tag{16}$$

or identical for equal conductances. We select $T_R = Q/(K_1 + K_2)$ such that with Eqs. (10) and (16) the flux boundary conditions, Eqs. (5), and Eq. (7) result in the nondimensional conditions

$$\frac{d\theta_1(0)}{dx_1} = -1, \qquad \frac{d\theta_1(1)}{dx_1} = \frac{K_2}{K_1} \tag{17}$$

Finally, substitution of Eq. (14) into Eq. (12) results in the scaled fin equation

$$\frac{d^2\theta_1}{dx_1^2} - \beta^2\theta_1 = 0 \tag{18}$$

where the radiation/conductance number is

$$\beta^2 = L_d P_1 \mathcal{F}_{12} h_r \left(\frac{1}{K_1} + \frac{1}{K_2}\right) = \frac{R_1 + R_2}{1/(L_d P_1 \mathcal{F}_{12} h_r)} \tag{19}$$

that is, the ratio of conductive resistance to radiative resistance. For equal conductances, Eq. (19) contracts to the familiar fin length parameter[7]:

$$\beta = L_d\sqrt{\frac{2\mathcal{F}Ph_r}{kA}} = L_d\sqrt{\frac{8\mathcal{F}h_r}{kd}} \tag{20}$$

In terms of these variables, Eq. (10) with Eqs. (14) and (15) yields the overall heat transfer rate Q and the defining equation for $\mathcal{E}$:

$$Q = \frac{(K_1 + K_2)(T_{d1} - T_{d2})}{1 + \theta_1(1) + \theta_2(1)} \equiv \mathcal{E}(K_1 + K_2)(T_{d1} - T_{d2}) \tag{21}$$

Thus the effectiveness factor is obtained from

$$\mathcal{E} = \frac{1}{1 + \theta_1(1) + \theta_2(1)} = \frac{1}{1 + \theta_1(1) + K_1\theta_1(0)/K_2} \tag{22}$$

Now, the general solution of Eq. (18) is

$$\theta_1 = A\cosh(\beta x_1) + B\sinh(\beta x_1) \tag{23}$$

so that with application of boundary conditions (17) we have

$$\theta_1(x_1) = \frac{K_2/K_1 + \cosh\beta}{\beta\sinh\beta}\cosh\beta x_1 - \frac{1}{\beta}\sinh\beta x_1 \tag{24}$$

Application of this result to Eq. (22) then yields the interpenetration-region effectiveness factor

$$\mathcal{E} = \frac{1}{\dfrac{2}{\beta\sinh\beta} + \dfrac{\kappa}{\beta\tanh\beta} + 1} \tag{25}$$

The limit of this factor as $\beta \to \infty$ (say, for arbitrarily small fiber diameters) is 1. Equation (21) shows that this limit corresponds to the sum of conductances in parallel, as if the fibers were connected at the ends to both sides of the interface.

Conversely, the overall rate of heat transfer in Eq. (21) may be expressed in terms of the conventional fin efficiency η,

$$Q \equiv \eta L_d P_1 \mathcal{F}_{12} h_r (T_{d1} - T_{d2}) \tag{26}$$

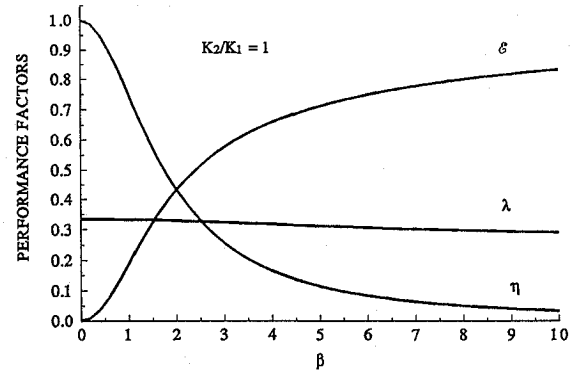

Fig. 3 Fiber performance factors.

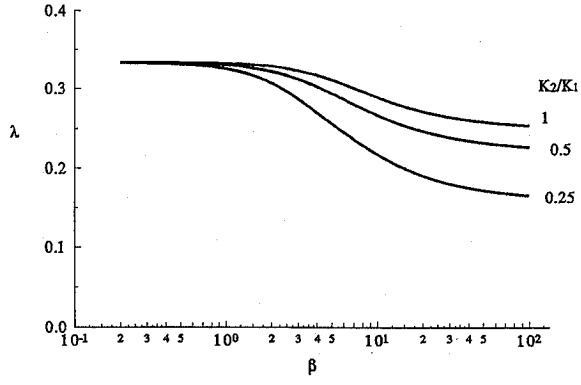

Fig. 4 Effective conduction-length ratio.

or, in terms of the effective conductance length $L_e = \lambda L_d$,

$$Q \equiv \frac{T_{d1} - T_{d2}}{\dfrac{L_e}{k_1 A_1} + \dfrac{1}{L_d P_1 \mathcal{F}_{12} h_r} + \dfrac{L_e}{k_2 A_2}} \tag{27}$$

By comparison of Eqs. (26) and (27) with Eqs. (21) and (25), it is found that

$$\eta = \frac{\mathcal{E}(\kappa + 2)}{\beta^2} = \frac{\kappa + 2}{\dfrac{2\beta}{\sinh\beta} + \dfrac{\kappa\beta}{\tanh\beta} + \beta^2} \tag{28}$$

and

$$\lambda = \frac{1}{\mathcal{E}(\kappa + 2)} - \frac{1}{\beta^2} = \frac{1}{\beta^2}\left(\frac{1}{\eta} - 1\right)$$

$$= \frac{1}{\kappa + 2}\left(\frac{2}{\beta\sinh\beta} + \frac{\kappa}{\beta\tanh\beta} + 1\right) - \frac{1}{\beta^2} \tag{29}$$

These three factors are shown in Fig. 3 for $K_2/K_1 = 1 (\kappa = 2)$.

The advantage of using λ is not only for convenient extension to partially interpenetrating interfaces, as noted previously,[6] but also that this fractional conductance length remains nearly constant for large variations in β, as seen in Fig. 3. Indeed, for $K_2/K_1 = 1$, λ varies from 1/3 at $\beta = 0$ to 1/4 at $\beta = \infty$, as in Fig. 4.

Overall Interface Conductance

For application of the preceding model we consider the effective conductance length as defined by Eq. (27). The interpretation of this equation is clear: Heat is conducted through type-1 fibers over an effective length of $L_e = \lambda L_d$, followed by radiation across surface area $L_d P_1$, and followed by conduction through type-2 fibers, with the three thermal resistances acting in series. Of course the actual heat exchange occurs continuously, as indicated in Fig. 2, but the effective result is the same as in this interpretation.

In applications it may not be possible or desirable to have the fiber interpenetration extend to the opposite side, but rather to have

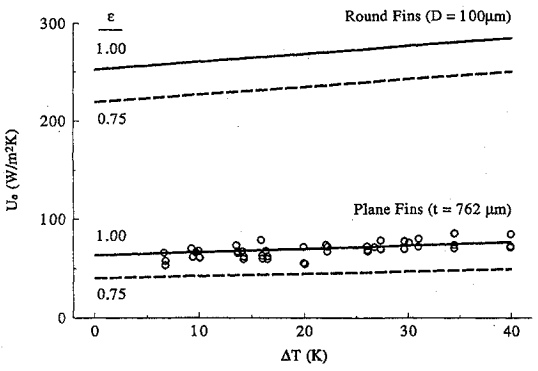

Fig. 5 Comparison of overall conductance with measurements of Peterson and Fletcher.[4]

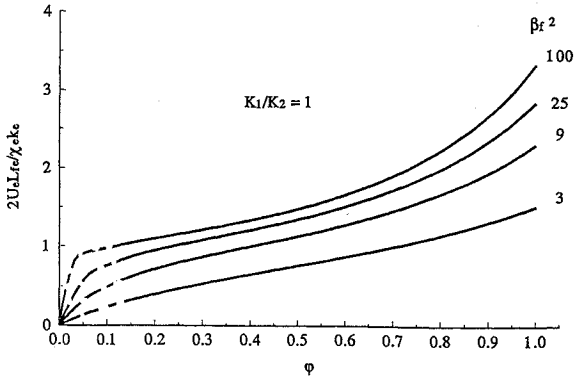

Fig. 6 Dependence of overall interface conduction on fiber penetration depth.

partial penetration, as shown in Fig. 2. This is accommodated in Eq. (27) by replacing L_e with $L_e + L_b = L_f - (1-\lambda)L_d$ for each side, and changing to the overall temperature difference so that $Q = (T_{b1} - T_{b2})/R_{\text{tot}}$, where

$$R_{\text{tot}} = \frac{L_{f1} - (1-\lambda)L_d}{k_1 A_1} + \frac{1}{L_d P_1 \mathcal{F}_{12} h_r} + \frac{L_{f2} - (1-\lambda)L_d}{k_2 A_2} \tag{30}$$

Let the volume fraction of fibers attached to substrate i be defined by $\chi_i \equiv V_{fi}/V_b = (A_i L_{fi})/(A_b L_{fi}) = A_i/A_b$. Then with the interface overall effective unit conductance U_e defined by $Q \equiv U_e A_b (T_{b1} - T_{b2})$, as in heat-exchanger theory, Eq. (30) results in

$$\frac{1}{U_e} = \left(\frac{1}{\chi_1 k_1} + \frac{1}{\chi_2 k_2}\right)[1 - (1-\lambda)\phi]L_{fe} + \frac{a_1/p_1}{\phi \chi_1 \mathcal{F}_{12} h_r L_{fe}} \tag{31}$$

where the effective fiber length is

$$L_{fe} = \frac{L_{f1}/\chi_1 k_1 + L_{f2}/\chi_2 k_2}{1/\chi_1 k_1 + 1/\chi_2 k_2} \tag{32}$$

and where $a/p = d/4$ for fibers, and $a/p = t/2$ for plane fins.

For equal properties and geometry of the two surfaces, the fully penetrated, the overall conductance from Eq. (31) becomes

$$U_e = \frac{h_r \chi}{2\lambda \dfrac{h_r L_f}{k} + \dfrac{1}{\mathcal{F}} \dfrac{a}{p L_f}} \tag{33}$$

Thus, the conductance is seen to increase with temperature through h_r, to increase with volume fraction, and to decrease with increasing size parameter a/p.

In Fig. 5, Eq. (33) is compared with measurements on plane fins 2 in. (50.8 mm) long and 0.030 in. (0.762 mm) thick, on a 0.25-in. (6.35-mm) pitch,[4] which yields a solid volume fraction of 0.12; ΔT is the substrate temperature difference. The experiments[4] were carried out with one substrate temperature held fixed at 273 K, so that the other substrate temperature was 273 K + ΔT and the average temperature was 273K + $\Delta T/2$; the material conductivity was $k = 40.06 + 0.32(273\text{K} + \Delta T/2)$ W/m · K. There is excellent agreement for near-blackbody surfaces; the emissivity of the experiments was not available, but its effect is shown by the dashed curves in Fig. 5. The increase in U_e with ΔT is the result of h_r increasing with the average temperature.

If the same material is now used as rods of the same length and volume fraction, but with a diameter of 0.1 mm, then the overall conductance increases by a factor of 5, as shown by the upper curves in Fig. 5; smaller carbon fibers would improve performance even more. Thus, there is a large potential for performance improvement with interpenetrating brush fibers.

Optimum Fin Length

It is seen in Eq. (31) that for every constant fiber diameter or thickness, and for constant fractional penetration, there is a value of L_{fe} that minimizes $1/U_e$ and thus maximizes the rate of heat transfer. Differentiating Eq. (31) with respect to L_{fe} and equating to zero, and keeping λ fixed because it is a slowly varying function, yields the fiber length for maximum Q:

$$L_{fe,Q} = \sqrt{\frac{a_1/p_1}{\phi \chi_1 \mathcal{F}_{12} h_r} \frac{k_e \chi_e/2}{1 - (1-\lambda)\phi}} \tag{34}$$

where the effective conductivity and volume fraction are

$$\frac{2}{\chi_e k_e} = \frac{1}{\chi_1 k_1} + \frac{1}{\chi_2 k_2} \tag{35}$$

Thus, the optimum length decreases as the inverse square root of the fiber diameter and with increasing h_r (temperature). This optimum length corresponds to the following value of β:

$$\beta_Q^2 = \frac{2\phi^2 L_{fe,Q}^2 \chi_1 \mathcal{F}_{12} h_r}{\chi_e k_e a_1/p_1} = \frac{\phi}{1 - (1-\lambda)\phi} \tag{36}$$

For $\phi = 1$ and $\lambda = 1/3$, $\beta_Q = 1/\sqrt{(\lambda)} = \sqrt{(3)}$. This corresponds to $\eta_Q = 1/2$ from Eq. (29) and agrees with previous findings.[7,8]

By contrast, for any fiber length, whether optimum or not, performance is uniformly improved by reducing the size of fiber for fixed volume fraction (see Fig. 5); this is seen by recasting Eq. (31) as

$$\frac{U_e L_{fe}}{k_e \chi_e/2} = \frac{\phi \beta_f^2}{1 + \phi \beta_f^2 [1 - (1-\lambda)\phi]}$$

$$\rightarrow \frac{1}{1 - (1-\lambda)\phi} \qquad \text{as} \quad \phi \beta_f^2 \rightarrow \infty \tag{37}$$

where

$$\beta_f = L_{fe} \sqrt{\frac{2\chi_1 \mathcal{F}_{12} h_r}{\chi_e k_e a_1/p_1}} = L_{fe} \sqrt{\frac{2\chi_2 \mathcal{F}_{21} h_r}{\chi_e k_e a_2/p_2}} \tag{38}$$

As the fiber diameter or thickness becomes arbitrarily small, β_f becomes unbounded, and the Biot number parameter U_e in Eq. (37) attains its maximum value depending on ϕ, as shown in Fig. 6.

A possible application of the interpenetrating fiber or fin interface is its use as an active control of the rate of heat transfer across the interface. As the fraction of interpenetration is increased, U_e increases to its limiting value, as indicated in Fig. 6. It is seen that the variation is nearly linear over a wide range of ϕ, which is advantageous for control systems. For very small fibers only a small change in substrate separation would result in a large effect on the rate of heat transfer.

Conclusions

An analysis has been carried out for a thermal interface with interpenetrating fibers from opposite sides of the interface, which is valid for close-packed fibers (or fins) either in vacuum or with an intervening conductive medium. The results show that there exists a fiber length (parameter-dependent) for optimum heat transfer, in agreement with previous work,[9,10] and that the thermal conductance

of the interface can approach that in the case where all fibers are attached to both substrates, provided the fibers are fine enough. Brush-fiber interfaces offer prospects for high-thermal-performance interfaces.

Acknowledgment

This work was performed under NASA Contract NAS9-18844 (NASA SBIR Phase 1).

References

[1]Peterson, G. P., Fletcher, L. S., and Blackler, D., "Thermal Performance of Thermal Pad Contact Heat Exchangers," *Journal of Thermophysics and Heat Transfer*, Vol. 6, No. 1, 1992, pp. 69–76.

[2]Peterson, G. P., and Fletcher, L. S., "Heat Transfer Enhancement Techniques for Space Station Cold Plates," *Journal of Thermophysics and Heat Transfer*, Vol. 5, No. 3, 1991, pp. 423–428.

[3]Stobb, C. A., and Limardo, J. G., "Overall Contact Conductance of a Prototype Parallel Fin Thermal Interface," AIAA Paper 92-2846, July 1992.

[4]Peterson, G. P., and Fletcher, L. S., "Radiant Heat Exchanger Test Report: Determination of the Thermal Contact Conductance and Adhesion Characteristics of Coldplate Thermal Test Pads," Rept. P.O. R97PLA-89271802, Texas A&M University, College Station, TX, April 1990.

[5]Siegel, R., and Howell, J. R., *Thermal Radiation Heat Transfer*, 2nd ed., McGraw–Hill, New York, 1981.

[6]Lund, K. O., "Radiation and Phase Change of Lithium Fluoride in an Annulus," *Journal of Thermophysics and Heat Transfer*, Vol. 7, No. 4, 1993, pp. 600–607.

[7]Incropera, F. P., and DeWitt, D. P., *Fundamentals of Heat and Mass Transfer*, 3rd ed., Wiley, New York, 1990.

[8]Lund, K. O., "Thermal-Contact Electronic Packaging in Solar-Pointing Space Environment," *Journal of Solar Energy Engineering*, Vol. 113, No. 1, 1991, pp. 42–50.

[9]Bartas, J. G., and Sellers, W. H., "Radiation Fin Effectiveness," *Journal of Heat Transfer*, Vol. 82, Feb. 1960, pp. 73–76.

[10]Lund, K. O., and Baker, K. W., "Minimum-Weight Analysis of Anisotropic Plane-Fin Heat-Pipe Space Radiators," *Journal of Solar Energy Engineering*, Vol. 115, No. 2, 1993, pp. 37–41.

K. J. Weilmuenster
Associate Editor